International Journal of Pharmaceutics: X 1 (2019) 100014

Contents lists available at ScienceDirect

International Journal of Pharmaceutics: X

journal homepage: www.journals.elsevier.com/international-journal-of-pharmaceutics-x

Preparation and characterization of Alendronate depot microspheres based on novel poly(-ε-caprolactone)/Vitamin E TPGS copolymers

Christina Koulouktsi[a], Stavroula Nanaki[a], Panagiotis Barmpalexis[b], Margaritis Kostoglou[c], Dimitrios Bikiaris[a,*]

[a] Laboratory of Polymer Chemistry and Technology, Department of Chemistry, Aristotle University of Thessaloniki, Thessaloniki 54124, Macedonia, Greece
[b] Department of Pharmaceutical Technology, School of Pharmacy, Aristotle University of Thessaloniki, Thessaloniki 54124, Macedonia, Greece
[c] Laboratory of General and Inorganic Chemical Technology, Department of Chemistry, Aristotle University of Thessaloniki, GR-541 24 Thessaloniki, Greece

ARTICLE INFO

Keywords:
Polycaprolactone
Vitamin-E TPGS
Aledronate
Microspheres
Controlled release
Long acting injectables

ABSTRACT

In the present study, new aledronate (AL) loaded microspheres were prepared with the use of polycaprolactone (PCL)/Vitamin E d-α-tocopheryl poly(ethylene glycol) 1000 succinate (TPGS) copolymers. Specifically, PCL-TPGS copolymers, prepared at several PCL to TPGS ratios (namely, 90/10, 80/20, 70/30 and 60/40 w/w) via a ring opening polymerization process, were characterized by intrinsic viscosity, proton nuclear magnetic resonance (^{1}H NMR), Fourier transform infrared spectroscopy (FTIR), X-ray diffraction (XRD), differential scanning calorimetry (DSC) and enzymatic hydrolysis. Results showed that as TPGS content increases the intrinsic viscosity of the copolymer (and hence, the viscosity-average molecular weight) is decreasing, while FTIR analysis showed the formation of hydrogen bonds between the −C═O of PCL and the −OH of TPGS. Additionally, XRD analysis indicated that the prepared copolymers were semi-crystalline in nature, while enzymatic hydrolysis studies showed that increasing TGPS content led to increasing copolymer hydrolysis. In the following step, AL drug-loaded microspheres were prepared via single emulsification process. Scanning electron microscopy (SEM) revealed the formation of coarse drug-loaded microspheres with particle size close to 5 μm, while XRD analysis showed that the API was amorphously dispersed only in the cases of high TPGS content. Furthermore, FTIR analysis showed that the API did not interact with the copolymer components, while *in vitro* drug release studies showed that increasing PCL content led to decreasing API release rate. Finally, analysis of the drug release profiles suggested that the API release mechanism was solely governed by the polymer matrix erosion.

1. Introduction

Bisphosphonates (BPs) are a class of active pharmaceutical ingredients (APIs) widely used in the treatment of several calcium- related diseases and metabolic bone related pathologies, such as osteoporosis and Paget's hyperkalemia disease (Fleisch, 2000; Kim et al., 2010). They are highly potent inhibitors of bone resorption due to their affinity to hydroxyapatite and suppression of osteoclast activity. Extensive research on BPs has shown that these APIs inhibit osteoclast activity and induce osteoclast apoptosis (Hughes et al., 1995; Mondal et al., 2012; Sahni et al., 1993).

Aledronate (AL), a nitrogen-containing bisphosphonate, is a well-known anti-resorptive API used as a sodium salt in the oral treatment of several bone disorders, such as tumor induced hypercalcemia, Paget's disease, inflammation- related bone loss and others (Bae and Park, 2015; Luo et al., 2018; Miyazaki et al., 2014; Nafea et al., 2007; Samdancioglu et al., 2006). AL mainly acts on osteoclasts, while several studies have indicated its ability to enhance the differentiation of bone marrow cells, mesenchymal stem cells or adipose stem cells into osteoblasts (Duque and Rivas, 2007; Nishikawa et al., 1996; Wang et al., 2010; Wu et al., 2014). Based on these properties, AL may also be used in the treatment of periodontal defects, malignant hypercalcemia and orthopedic reconstruction (Samdancioglu et al., 2006; Sharpe et al., 2001). Novel studies, using Alendronate to prevent breast cancer bone metastasis, showed that it was an effective therapeutic drug and that it possesses antitumor and anti-angiogenic activities (Dong et al., 2018; Miller et al., 2013). Although AL's use in bone-related diseases is well established and its effectiveness in bone metastasis shows promising results, several problems associated with its low bioavailability (below 1%) and serious gastrointestinal side effects (esophageal irritation, ulcers, acid reflux, gastritis etc.) necessitate the preparation of a more sophisticated AL drug delivery system (Bae and Park, 2015; Kim et al.,

* Corresponding author.
E-mail address: dbic@chem.auth.gr (D. Bikiaris).

https://doi.org/10.1016/j.ijpx.2019.100014
Received 25 March 2019; Received in revised form 18 April 2019; Accepted 21 April 2019
Available online 25 April 2019

2010; Lin, 1996; Lin et al., 1994; Luo et al., 2018; Mondal et al., 2012; Rhim et al., 2009; Wu et al., 2014).

In an attempt to overcome these limitations, several approaches include the use of AL conjugated complexes with small APIs or proteins and the development of novel targeted drug delivery systems (Ezra et al., 2000; Luo et al., 2018; Wright et al., 2006). Especially, in the latter case, the use of a specialized systems able to deliver the API directly into the bone (targeted delivery), while simultaneously prolonging its action, seems to be a promising approach in order to provoke all AL's orally induced side effects. Recent attempt made in this directions include the development of liposomes, nano- and microparticles, transdermal devices, implants, pharmaceutical biodegradable cements etc. (Dolci et al., 2019; Gaba et al., 2015; Hosny, 2016; Luo et al., 2018; Qu et al., 2018; Yang et al., 2016). Out of them, the most promising approach in terms of production efficiency, regulatory registration pathway and scalability, seems to be the use of suitable biodegradable polymeric materials for the preparation of injectable AL depot microspheres. Advantages of such drug delivery systems include good biocompatibility, high drug encapsulation efficiency, proper particle size characteristics (which enables the incorporation of the treatment into the bone defected area), tunable drug release profiles and ease of application (Kim et al., 2010; Luo et al., 2018; Mondal et al., 2012; Nafea et al., 2007; Samdancioglu et al., 2006). Recent scientific attempts made in this direction include the use of polylactic acid, poly (lactic-co-glycolic acid), polymethacrylates, calcium phosphate, poly(b-hydroxybutyrate-co-b-hydroxyvaleate), poly(D,L-lactic acid)-block-poly(ethylene glycol) and poly (lactic-co-caprolactone) (Bae and Park, 2015; Balas et al., 2006; Luo et al., 2018; Nafea et al., 2007, 2018; Umeki et al., 2010).

One promising biodegradable polymer used widely in the preparation of depot microsphere systems is poly(-ε-caprolactone) (PCL). PCL is a semicrystalline flexible polymer with low melting temperature (~60 °C), low glass transition temperature (~ −60 °C), appropriate mechanical properties, and good solubility in several solvents (Nanaki et al., 2011). Despite its important advantages, PCL's high degree of crystallinity and hydrophobicity reduces extensively its compatibility with soft tissues and lowers its in vivo biodegradability (Nerantzaki et al., 2018; Siafaka et al., 2016; Zhang et al., 2015). Hence, in order to overcome these limitations, several attempts have been made to prepare new PCL-based copolymers by adding compounds with higher biodegradation rates (compared to PCL), which eventually will lead to microspheres with tunable biodegradation rate, and hence, tunable API release (Bikiaris et al., 2008; Harada et al., 2008; Nanaki et al., 2011; Yuan et al., 2000; Zorba et al., 2007). One such, highly promising compound suitable for the preparation of AL depot microspheres for the treatment of tumor induced hypercalcemia, is Vitamin E d-α-tocopheryl poly(ethylene glycol) 1000 succinate (TPGS). TPGS is synthetic water-soluble derivative of natural vitamin E available as a white to light-brown, waxy solid (Zhang et al., 2012). It is a mixture composed principally of monoesterified polyethylene glycol 1000, the diesterified polyethylene glycol 1000, free polyethylene glycol 1000 and free tocopherol (Yang et al., 2018; Zhang et al., 2012). It is widely used in the preparation of pharmaceutical formulation products as an absorption enhancer, antioxidant, emulsifying agent, granulation aid, ointment base, solubilizing agent, surfactant, suspending agent, and tablet binder (Guo et al., 2013). Additionally, recent studies on TPGS has shown that it can act as an anticancer agent, which induces apoptogenic activity against many cancer types (Neuzil et al., 2007), while exhibiting non-toxicity to normal cells and tissues (Yang et al., 2018). Therefore, the addition of TPGS not only will improve the biodegradation properties of PCL, but will simultaneously offer anticancer properties into the system, something that was only recently acknowledged via the preparation of genistein loaded TPGD-b-PCL nanoparticles (Zhang et al., 2015).

Hence, the objective of the present study is to evaluate the use of novel PCL-TPGS copolymers in the preparation of a new AL injectable microsphere depot formulation. As in the case of many other BPs, AL preparation in the form of biodegradable microspheres is related to problems associated to low drug encapsulation efficiency and extensive initial burst release (Bae and Park, 2015; Miladi et al., 2013). Therefore, the development of a new AL sophisticated biodegradable microsphere depot, based on PCL-TPGS copolymers, that will be able to simultaneously prolong API's release in the site of action, improve its stability and enhance its pharmacological activity (due to the anticancer properties of TPGS), will be highly beneficial for the treatment of tumor induced hypocalcemia defects.

2. Material and methods

2.1. Materials and reagents

Vitamin E TPGS (TPGS; purum 99.5%), ε-caprolactone (ε-CL; purum 99%), stannous octoate ($Sn(Oct)_2$; purum 95.0%) and poly(vinyl alcohol) (PVA; hydrolyzed 87%-89%, having Mw between 13,000 and 23,000) were purchased from Sigma-Aldrich (Sigma-Aldrich Corporation, St Louis, MO). ε-CL was distilled at 94 °C–95 °C under reduced pressure at about 5 mmHg prior to use in order to remove the inhibitor contained within. *Rhizopus delemar* and *Pseudomonas cepacia* lipases were purchased from BioChemika. AL API was kindly donated by Pharmathen S.A. All other chemicals and reagents were of analytical grade.

2.2. Synthesis and purification of PCL and PCL-TPGS copolymers

Synthesis of PCL-TPGS was performed by ring opening polymerization as described previously (Zhang et al., 2015). Briefly, accurately weighted amounts TPGS corresponding to weight ratios of ε-CL to TPGS of 90/10, 80/20, 70/30 and 60/40 w/w, respectively, were placed at round-bottomed flask, purged with dry nitrogen three times, equipped with mechanical stirrer and vacuum apparatus (1–2 Torr). After one (1) hour of mixing at 140 °C accurately weighted amounts of ε-CL were added along with appropriate stannous octoate concentrations and the blend was mixed at 140 °C for 24 h under nitrogen atmosphere. Polymerization (Fig. 1) was stopped after cooling to room temperature. The resulting copolymers were dried in a vacuum oven at 30 °C. For the purification of copolymers, 3 g of the biomaterial were placed in 50 mL of acetone and mixed until complete solubilization. Then, 350 mL of H_2O were added and the resultant precipitates was collected via filtering (washed three times with H_2O in order to remove any remaining residuals). The resultant purified copolymers were dried in a vacuum over and stored in desiccators before further use.

2.3. Preparation of microspheres

AL loaded PCL-TPGS microspheres were prepared based on the solvent evaporation/ extraction method (Nanaki et al., 2018a,b). Briefly, 100 mg of PCL-TPGS (at different weight ratios) were dissolved in six (6) mL of CH_2Cl_2 and then, 10 mg of AL were dispersed with the aid of a probe sonicator (model UP50H; Hielscher Ultrasound Technology). The resultant dispersion was added dropwise in 18 mL of PVA aqueous solution, 1% w/v in concentration, and the mixture was emulsified at 30,000 rpm using Ultra Turrax (IKA, Staufen im Breisgau, Germany). Then, the emulsion was added to 200 mL H_2O and left under constant magnetic stirring for 24 h, where the organic phase was totally removed. The prepared miscospheres were collected via centrifugation at 4500 rpm for 20 min and washed three times in order to remove any excess or surface located API. After washing, the microspheres were lyophilized and placed in desiccator till further use. MPs without the use of API were also prepared for comparison. The preparation was exactly the same without the addition of the API in the organic solvent solution.

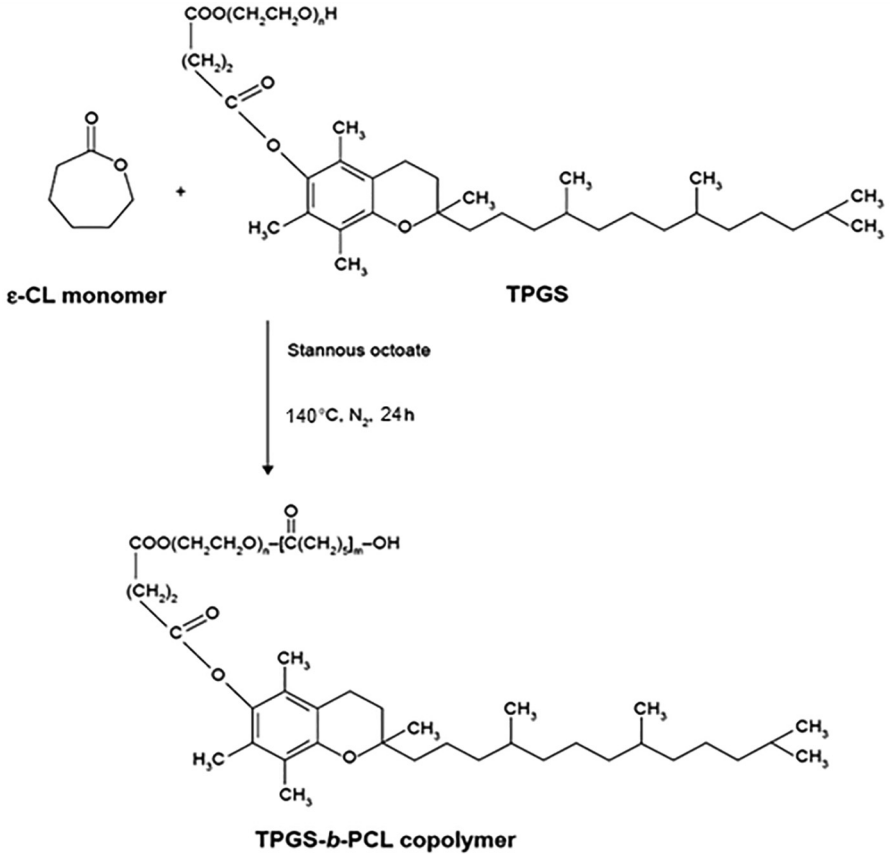

Fig. 1. Polymerization reaction for the preparation of the PCL-TPGS copolymers.

2.4. Intrinsic viscosity

Intrinsic viscosity [η] measurements of the prepared PCL-TPGS copolymers were performed at 25 °C using Ubbelohde viscometer. Each polymer was dissolved in chloroform at final concentration 1% w/v. and filtered through a disposable membrane filter (0.2 mm, Teflon). Intrinsic viscosity was calculated using the Solomon-Ciuta equation (Solomon and Ciută, 1962):

$$[\eta] = ([2(t/t_0 - -ln(t/t_0) - -1)]^{1/2})/c \quad (1)$$

where, c is the concentration of the solution, t the flow time of solution, and t_0 the flow time of pure solvent.

Based on the measured intrinsic viscosity values the copolymer viscosity-average molecular weight was estimated using the Mark–Houwink–Sakurada (MHS) equation:

$$[\eta] = KMv^a \quad (2)$$

where, Mv the viscosity-average molecular weight, and K and a, are the constants for a given solute–solvent system. In the present study a and K values were set as 0.6021 and 1.09×10^{-3} dLg^{-1} respectively.

2.5. Nuclear magnetic resonance (^{1}H NMR)

^{1}H NMR images of the prepared PCL-TPGS copolymers were obtained using a Bruker spectrometer (Bruker, Billerica, MA) operating at a frequency of 400 MHz. Deuterated chloroform ($CDCl_3$) was used as a solvent in polymer solutions at final concentration 5% w/v, and the spectra were internally referenced to tetramethylsilane. The number of scans was 10, and the sweep width was 6 kHz.

2.6. Enzymatic hydrolysis

The enzymatic hydrolysis test was performed based on a previously employed method of ours (Nanaki et al., 2018a). Briefly, neat PCL and PCL-TPGS copolymers in the form of films ($10 \times 20 \times 0.4$ mm^3, ~100 mg) were prepared using an OttoWeber Type PW 30 hydraulic press as described earlier. The films were placed in perti dishes, wherein 5 mL of phosphate buffer solution (0.2 M, pH 7.4) was added, containing 0.09 mg/mL Rhizopus delemar lipase and 0.01 mg/mL Pseudomonas cepacia lipase. The petri dishes were kept at 37.0 °C ± 1.0 °C in an oven for four (4) days, while the media were replaced every 24 h. After a predetermined time intervals the films were removed from the lipase solution, washed thoroughly with distilled water and dried at 30 °C under vacuum, till constant weight. Every measurement was repeated three times. The degree of enzymatic hydrolysis was estimated from mass loss.

2.7. Fourier-transformed infrared spectroscopy (FTIR)

The chemical structure of the neat materials, synthesized copolymers and prepared microspheres was determined with the use of FTIR spectroscopy. FTIR spectra of the samples were received with an FTIR spectrometer (model FTIR-2000, Perkin Elmer, Dresden, Germany) using KBr discs (thickness of 500 μm). The spectra were collected in the range from 4000 to 400 cm^{-1} at a resolution of 2 cm^{-1} (total of 64 co-added scans) were baseline corrected and converted into absorbance mode.

2.8. Wide angle X-ray diffractometry

X-ray powder diffraction (XRD) patterns of copolymers were recorded using an XRD-diffractometer (Rigaku-Miniiflex II) with a CuKα

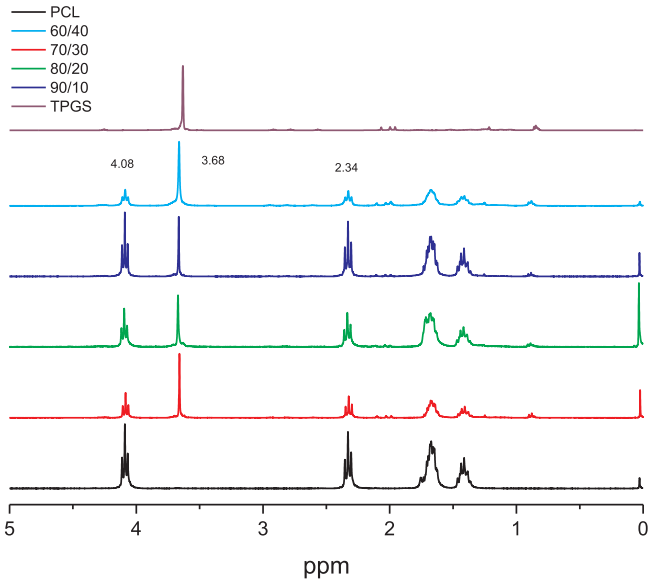

Fig. 2. ^{1}H NMR spectra of neat PCL and PCL-TPGS copolymers.

radiation for crystalline phase identification (λ = 0.15405 nm for CuKα). The sample was scanned from 5 to 30° (for copolymers) and 5 to 45° (for microspheres).

2.9. Differential scanning calorimeter (DSC)

Differential scanning calorimeter (DSC) study performed using a Perkin–Elmer, Pyris Diamond DSC, calibrated with Indium and Zinc standards. In the case of neat copolymers, samples of 5.0 ± 0.1 mg sealed in aluminium pans were heated 50 °C above their melting point at a heating rate of 20 °C/min under nitrogen atmosphere and held at that temperature for 5 min. Then the samples were supercooled to −75 °C at a cooling rate of 200 °C/min held at this temperature for 1 min and subsequently heated again with 20 °C/min in order to record the melting temperature (Tm) and glass transition temperature (Tg). In the case of drug-loaded microspheres, samples of 5.0 ± 0.1 mg sealed in aluminium pans were heated from 0 °C to 200 °C at heating rate of 20 °C/min under nitrogen atmosphere.

2.10. Scanning electron microscopy (SEM)

The size and the morphology of the microspheres were determined using scanning electron microscopy (SEM). Specifically, the prepared microspheres covered with a carbon coating to provide good conductivity of the electron beam were examined by a SEM JEOL 6000. Operating conditions were the following: accelerating voltage 20 kV, probe current 45 nA, and counting time 60 s.

2.11. Yield, encapsulation efficiency and drug loading

MPs' yield, drug loading and encapsulation efficiency (EE) were determined by applying the following equations:

$$\text{Yield } (\%) = [\text{weight of microspheres}] / [\text{initial weight of polyesters and AL}] \times 100 \quad (3)$$

$$\text{Drug loading}(\%) = [\text{weight of drug in microspheres}] / [\text{weight of microspheres}] \times 100 \quad (4)$$

$$\text{EE } (\%) = [\text{weight of PTX in nanoparticles}] / [\text{initial weight of PTX}] \times 100 \quad (5)$$

2.12. High performance liquid chromatography (HPLC)

AL content in the prepared samples was performed by high-performance liquid chromatography on a Shimadzu Prominence HPLC system consisted of: degasser (Model DGU-20A5), pump (Model LC-20AD), manual injector with a 100 μL loop (Model Rheodyne, Cotati, CA, USA), variable infrared detector (RID), and column oven (Model CTO-20AC). Chromatographic analyses were done on an Allsep Anion analytical column C18 (7 μm particle size, 150 mm × 4.6 mm I.D.). The entire HPLC analysis was performed using LC solutions software, v. 1.21 SP1 (Shimadzu Corporation, Kyoto, Japan) isocratically, with a flow rate of 0.9 mL/min, while the temperature was set at 35 °C and the volume injected into the chromatographic system was 100 μL. Mobile phase consisted of H_2O with 0.5 mL/L formic acid (pH 3.8 adjusted with NaOH 5 N).

2.13. In vitro release test

In vitro API release studies were conducted in a shaking incubator device (Memmert GmbH + Co. KG, Schwabach, Germany). Briefly, accurate amounts of drug-loaded microspheres were inserted in regenerated cellulose dialysis tubing (SERVAPOR dialysis tubing, MWCO 12,000–14,000) and added in testing tubes containing 100 mL of Phosphate Buffer Salline (PBS, pH 7.4) and incubated at 37 °C for several days. In predetermined time intervals 1.0 mL of sample was removed, filtered and analyzed via the HPLC method described in the previous section. Freshly prepared PBS equilibrated at 37 °C was used as replacement media.

3. Results and discussion

3.1. PCL-TPGS copolymer characterization

3.1.1. ^{1}H NMR analysis

^{1}H NMR was used in order to evaluate the PCL-TPGS synthetic process (Fig. 2).

Figure analysis showed several typical signals corresponding to the neat PCL. Specifically, the characteristic multiple peak located at 1.30–1.40 is attributed to methylene group c, the peak at 1.58–1.66 is attributed to methylene group b, the triple peak at 2.26–2.31 corresponds to the methylene d next to carbonyl group, while the triple peak at 4.02–4.08 is attributed to the methylene group a, standing next to oxygen atoms (Nanaki et al., 2011). Further analysis of the PCL-TPGS copolymer spectra, showed additional peaks in all spectra located at 3.68, 1.61–1.71 and 1.34–1.44 ppm, corresponding the –CH_2, the –CH_2-(4H) and the -CH_3(2H) protons of TPGS, respectively. Al these peaks are in accordance with previous studies regarding TPGS (Ciardelli et al., 2005). Hence, the presence of these specific NMR peaks certifies the successful synthesis of PCL-TPGS copolymers.

The compositions of copolymers were calculated by ^{1}H NMR and the results are presented in Table 1. Evidently, the calculated weight ratios are almost identical with the theoretical ones, taking into account the feeding ratios, providing evidence for the appropriateness of the procedure used.

Table 1
Theoretical and calculated compositions, intrinsic viscosity, [η], values and viscosity-average molecular weights, Mv, of prepared PCL-TPGS copolymer.

Sample	%wt	%wt ^{1}HNMR	[η] (dL/g)	Mv (g/mol)
PCL-TPGS, 90/10	90/10	93.3/6.7	0.32	4191
PCL-TPGS, 80/20	80/20	83.2/16.8	0.21	1924
PCL-TPGS, 70/30	70/30	68.9/31.1	0.14	1035
PCL-TPGS, 60/40	60/40	62.5/37.5	0.10	778

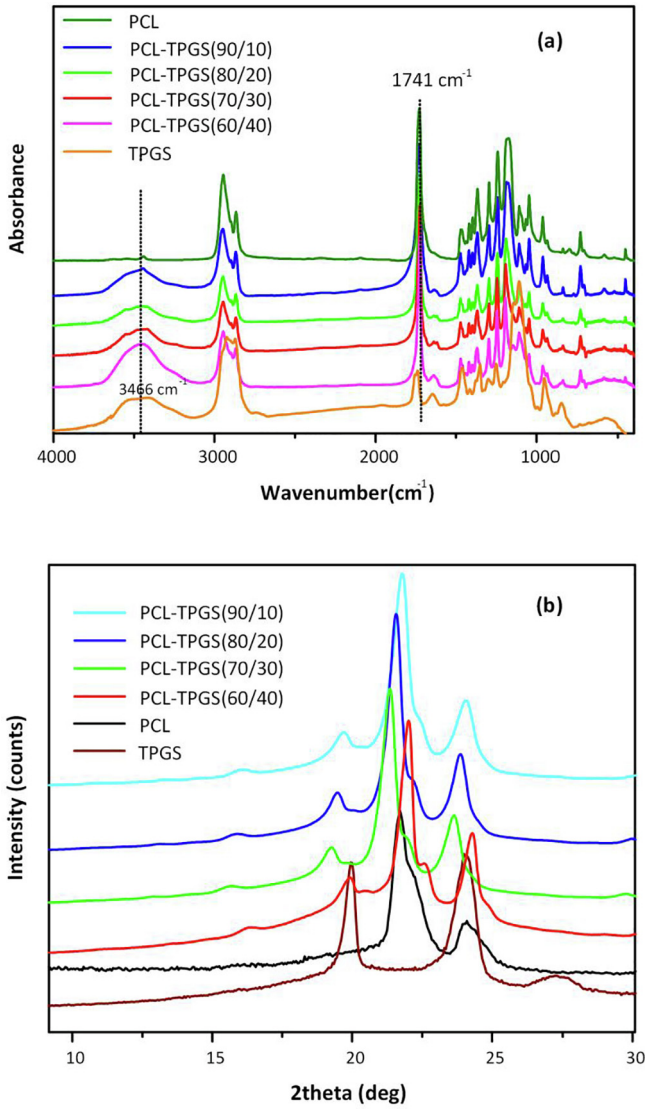

Fig. 3. FTIR spectra (a) and powder x-ray diffractograms (b) of neat PCL, neat TPGS and PCL-TPGS copolymers at several weight ratios.

3.1.2. Intrinsic viscocity analysis

Intrinsic viscosity (η) results, along with the estimated viscosity-average molecular weights (Mv) are presented in Table 1. Specifically, η values of 0.32, 0.21, 0.14 and 0.10 dL/g, and Mv values of 4191, 1924, 1035 and 778 g/mol, were obtained for the PCL-TPGS copolymers having a 90/10, 80/20, 70/30 and 60/40 wt ratio of PCL to TPGS, respectively. Results showed that as TPGS content increased the intrinsic viscosity of the copolymer (and hence, the Mv values) was decreased. This can be attributed to the increasing availability of TPGS hydroxyl groups that participate in the ring opening procedure of ε-CL, leading to a relatively fast reduction of ε-CL monomers and hence, to macromolecules of reduced molecular weight.

3.1.3. FTIR analysis

In a further step, FTIR analysis was used in order to identify whether intermolecular interactions are involved during the synthetic polymerization process of PCL-TPGS (Fig. 3(a)). In the case of neat PCL, figure analysis revealed characteristic IR peaks at 1741 cm^{-1}, corresponding to C=O, and in the region of 1000 to 1500 cm^{-1}, corresponding to C-C, C-H and C-O groups of the neat PCL polymer. In the case of neat TPGS, FTIR analysis showed a characteristic carbonyl ester FTIR peak at approximately 1730 cm^{-1}, i.e. at lower wavelengths compared to the C=O of PCL probably due to presence of intermolecular and intramolecular hydrogen bonds among the hydroxyl groups of PEG, while another characteristic FTIR peak for TPGS is observed at 1634 cm^{-1}, corresponding to the unsaturated bonds (C=C) present in the vitamin E molecule. Additionally, the FTIR peak observed at 3455 cm^{-1} is due to the presence of terminal hydroxyls in the molecule of TPGS. In the case of PCL-TPGS copolymers, FTIR analysis showed all characteristic peaks from both compounds, however, the IR peaks corresponding to the carbonyl groups of PCL and the –OH of TPGS were shifted in lower wavenumbers indicating the presence of intermolecular interactions between the components, a proof that the two compounds are interacting in order to form a new copolymer, and do not remain as a separate physical mixture.

3.1.4. XRD analysis

Fig. 3(b) shows the x-ray diffractograms of the neat PCL, neat TPGS and the PCL-TPGS copolymers at several weight ratios. Results showed that PCL, although is a semi-crystalline compound it has a high degree of crystallinity with characteristic XRD peaks at 2θ of 21.11°, 21.53° and 23.23°, respectively. Additionally, neat TPGS showed two strong XRD peaks at 2θ of 19.0° and 23.15°, while an additional small amorphous halo, observed in TPGS's diffractogram, verifies the semi-crystalline nature of this compound. In the case of PCL-TPGS copolymers, XRD diffractograms showed that in all weight ratios the copolymers were semi-crystalline in nature, with characteristic XRD peaks observed at 2θ of 15.96°, 19.38°, 21.58° and 23.88° respectively. Additionally, results showed that as the TPGS content increases the XRD amorphous halo increases, indicating that the amorphous part of the semi-crystalline PCL-TPGS copolymers increases too.

3.1.5. DSC analysis

Fig. 4(a) shows the DSC thermograms of the neat components and the prepared PCL-TPGS copolymers at several weight ratios. In the case of neat PCL one endothermic melting peak was observed at 64.21 °C, with no other thermal events, while in the case of neat TPGS the two endothermic melting peaks observed at 32.56 and 43.21 °C, respectively, verified its crystalline nature. In regards to PCL-TPGS copolymers, a single endothermic peak (located in between the melting temperatures of the neat components) was observed in all cases, indicating that the copolymerization process followed leads to the formation of crystalline copolymers. Additionally, DSC result revealed that increasing TPGS concentration leads to decreasing copolymer melting temperature, with Tm values of 62.07, 59.63, 56.44 and 52.02 °C for 90/10, 80/20, 70/30 and 60/40 PCL to TPGS ratio, respectively.

3.1.6. Enzymatic hydrolysis analysis

In a further step, the effect of TPGS on the enzymatic hydrolysis of PCL was evaluated in solutions containing a mixture of *R. delemar* and *Pseudomonas Cepacia* lipases, at 37 °C and pH 7.4. Results in terms of weight loss vs time are shown in Fig. 4(b). In the case of neat PCL the enzymatic hydrolysis was too slow with only a small percentage of mass lost (~1–2%) within the four (4) days tested. In general, enzymatic degradation of polyesters such as PCL is affected by several factors related to the chemical structure, the hydrophilic/hydrophobic balance among segments, the molecular weight, the frequency of ester bonds along the macromolecular chains, the degree of crystallinity, crystal's morphology and size, melting point, glass transition temperature etc. (Abou-Zeid et al., 2004; Bikiaris et al., 2012; Gan et al., 2001; Marten et al., 2003; Qiu et al., 2003).

Hence, in the present study the low enzymatic hydrolysis of the neat PCL was expected, since the polymer is highly hydrophobic, with high degree of crystallinity and a rather high melting point (compared to the 37 °C where hydrolysis occurs in the human body). In contrast to the neat PCL, the newly prepared PCL-TPGS copolymers showed substantially higher degree of enzymatic hydrolysis. Specifically, all tested PCL-TPGS showed a rather stable mass loss (~10–12%) in the first two

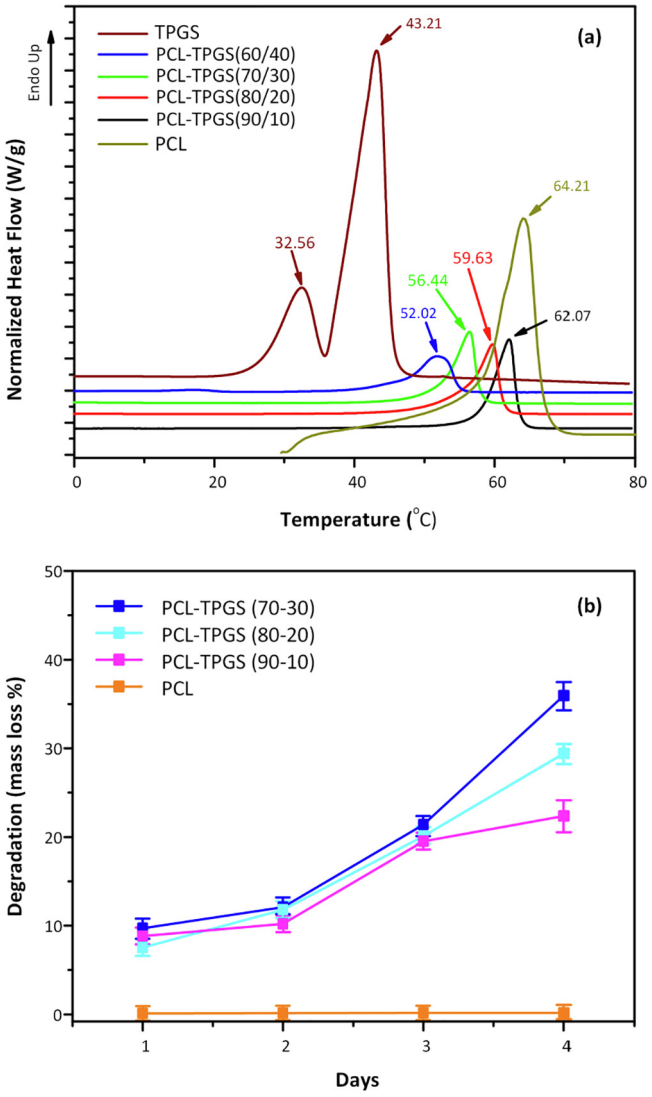

Fig. 4. DSC thermograms for neat PCL, neat TPGS and PCL-TPGS copolymers (a), and enzymatic hydrolysis results for neat PCL and PCL-TPGS copolymers (b).

days, followed by a sharp increase in the third day, with approximately 18–20% of total copolymer mass loss. After that point, results showed an increase in the degradation rate (and extent) as the content of TPGS increases, with PCL-TPGS 70/30, 80/20 and 90/10 w/w showing a total mass loss of approximately 38%, 27% and 22%, respectively. This behavior may be attributed to the amphiphilic/water-soluble nature of TPGS and the increase of the amorphous part of PCL-TPGS copolymers with increasing TPGS content.

3.2. Microspheres characterization

3.2.1. SEM analysis

In the present study, new PCL-TPGS copolymers at several weight ratios were evaluated for the preparation of AL microspheres. Initially, the effect of TPGS content on the size and morphological characteristics of neat placebo microspheres (microspheres without the incorporation of API) was evaluated. SEM analysis in Fig. 5 revealed that increasing PCL content in the copolymer, leads to increasing microparticle size, while more spherical shaped and uniform size distributions are also obtained. Specifically, in the case of placebo neat microparticles with high TPGS content (i.e. PCL-TPGS 60/40 and 70/30 w/w), particles with d50 values of less than 2–3 μm were obtained with high degree of agglomeration, in contrary to microparticles prepared with low TPGS content (i.e. PCL-TPGS 80/20 and 90/10 w/w), where uniform spherical shaped particles were obtained with d50 values of ~4–5 μm. This behavior can be attributed to the hydrophobic nature of PCL which lead to better homogenization and solvent extraction process.

SEM micrographs of drug-loaded microspheres prepared using the newly developed PCL-TPGS copolymers, revealed the formation of coarser microspheres with increased particle size compared to placebo (no API containing) microspheres (Fig. 5). This increased particle size and the irregular shape of the drug-loaded microspheres can be attributed to the API's solid physical state during the emulsification process, which provided the nucleation seeds for the microparticles formation. Additionally, comparison of the high PCL drug-loaded and placebo (no API) microspheres revealed the formation of less uniformed shaped particles, probably due to irregularities in the particle size distribution of the neat API, which in turn led to irregular shaped microspheres.

3.2.2. FTIR analysis

FTIR analysis was contacted in order to evaluate for possible molecular interactions between the API and the used PCL-TPGS copolymers. In the case of AL, results in Fig. 6(a) show a characteristic peak at 926 cm^{-1} corresponding to the hydroxyl group bending vibration of the API, while the peaks observed in the region of 1140 to 1320 cm^{-1} are due to P=O stretching. Additionally, a characteristic FTIR peak corresponding to API's N–H bending was recorded at 1645 cm^{-1}. In the case of AL-loaded microspheres, small changes were observed; the peaks at 1400 and 1382 cm^{-1} attributed to AL were shifted at 1419 and 1398 cm^{-1} showing that hydrogen bonds were probably formed during microparticles' formulation procedure. No new peaks were observed in microparticles showing that no chemical bonds were formed between the two components (API and copolymers) during the emulsification process.

3.2.3. DSC analysis

In a further step, the thermal properties and the physical state of the API in the prepared drug-loaded microspheres were evaluated via DSC. As it can be seen from Fig. 6(b) the DSC thermogram of AL shows a sharp endothermic peak at 135.37 °C corresponding to its melting peak, while all DSC thermograms of drug-loaded microspheres showed only the melting endotherms of the copolymers, indicating that the API is probably amorphously dispersed within the prepared system. However, since the in-situ AL amorphization within the copolymer melt during the DSC measurement cannot be excluded, the physical state of the API will be more thoroughly evaluated in the next section (XRD analysis). What is important to note is the two melting endotherms observed in the case of copolymers having high PCL content (PCL-TPGS 90/10 w/w) which may be attributed to different crystal formation of PCL as reported in similar studies (Nanaki et al., 2011).

3.2.4. XRD analysis

Since the API in-situ amorphization cannot be excluded in the DSC measurements, API's true physical state in the prepared PCL-TPGS microspheres was evaluated with the aid of XRD analysis (Fig. 7(a)). Results, showed that neat AL is a high crystalline API with several characteristic XRD peaks at 2θ of 9.40, 12.50, 13.65, 19.85, 25.05, 30.15 and 31.4 deg., respectively, while in regards to drug-loaded microspheres XRD patterns of high TPGS content (PCL-TPGS 60/40 w/w) showed a sharp XRD peak at 25.05 deg., indicating the API was dispersed in crystalline state within the prepared microsphere. In contrary, the rest prepared microspheres did not show any XRD peaks corresponding to the API, indicating AL is probably dispersed in amorphous state.

3.2.5. Microsphere yield and drug loading

Microspheres yield and drug loading are given in Table 2. Results

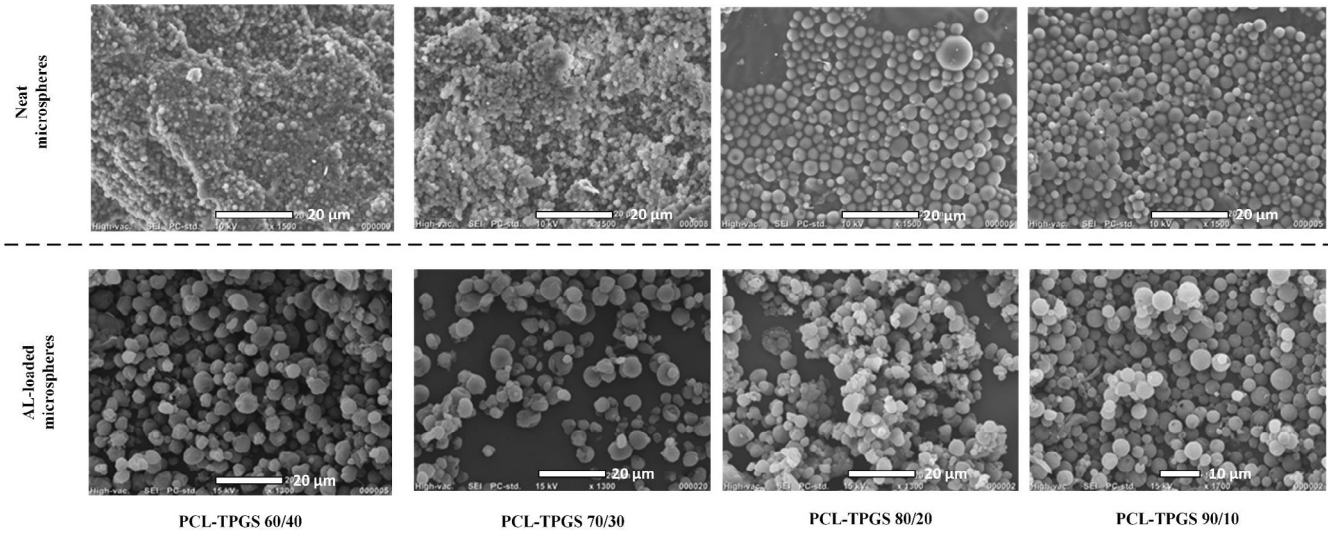

Fig. 5. SEM micrographs of neat (without API) and drug (AL) loaded polymeric PCL-TPGS microspheres.

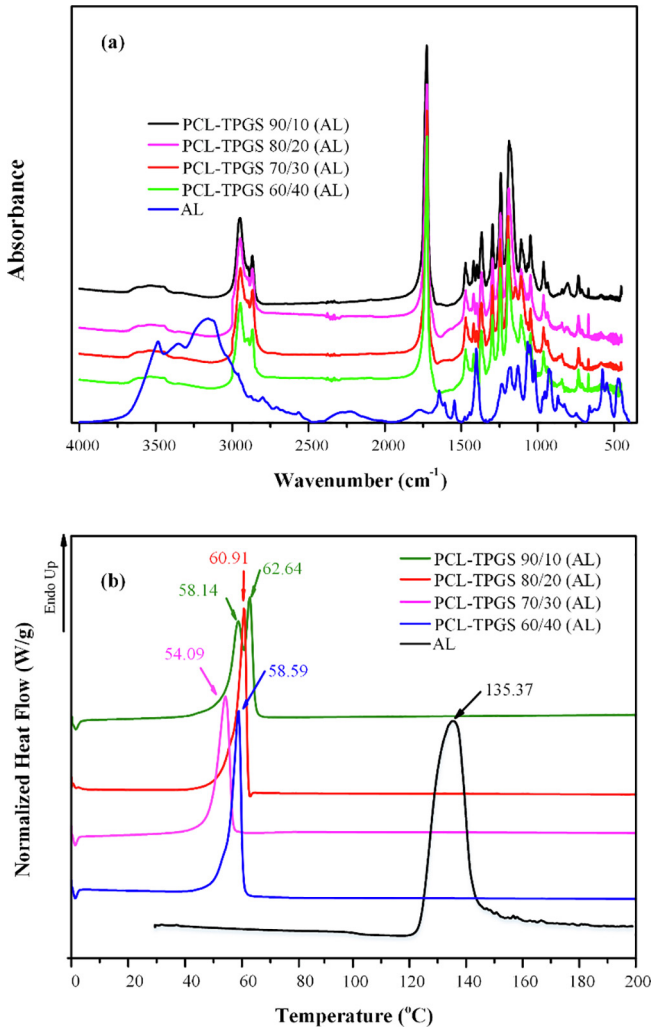

Fig. 6. FTIR spectra (a) and DSC thermograms (b) of AL drug-loaded microspheres.

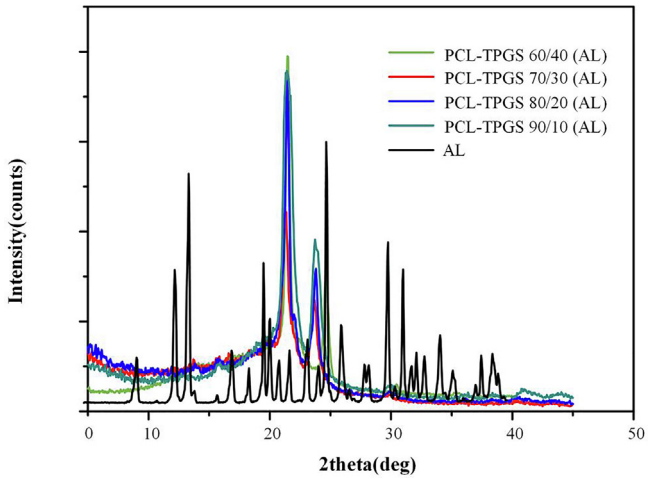

Fig. 7. XRD diffractograms of AL drug-loaded microspheres.

Table 2
AL drug-loaded microspheres yield and drug loading.

Sample	Yield (%)	Drug loading (%)	EE (%)
PCL-TPGS, 90/10 (AL)	67.05 ± 2.0	9.07 ± 1.2	66.89 ± 1.2
PCL-TPGS, 80/20 (AL)	65.83 ± 1.9	8.92 ± 1.0	64.59 ± 1.1
PCL-TPGS, 70/30 (AL)	61.77 ± 1.9	8.54 ± 1.1	58.03 ± 1.0
PCL-TPGS, 60/40 (AL)	50.45 ± 1.8	7.02 ± 0.9	38.95 ± 1.0

show yields above 50% in all cases, while increasing PCL content led to increasing microspheres yield, with maximum yield obtained in the case of PCL-TPGS 90/10 w/w microspheres (67.05%). Regarding drug loading and EE, similar results were obtained with increasing PCL leading to increasing drug loading and EE values. In general, this behavior may be attributed to the more hydrophobic nature of PCL, which results in more stable oil/water emulsions, sustaining thus the API within the formed droplet, not allowing it to escape into the extraction liquid.

3.2.6. *In vitro release analysis*

Fig. 8 shows the *in vitro* release profiles of all AL-loaded PCL-TPGS microspheres.

Results clearly show that increasing PCL content led to decreasing API's release rates. Specifically, in the case of microspheres prepared from PCL-TPGS copolymer in a ratio of 60/40 w/w, a rather fast release rate was observed with more than 90% of the API being released within the first seven (7) days. In contrary, microspheres having a high PCL

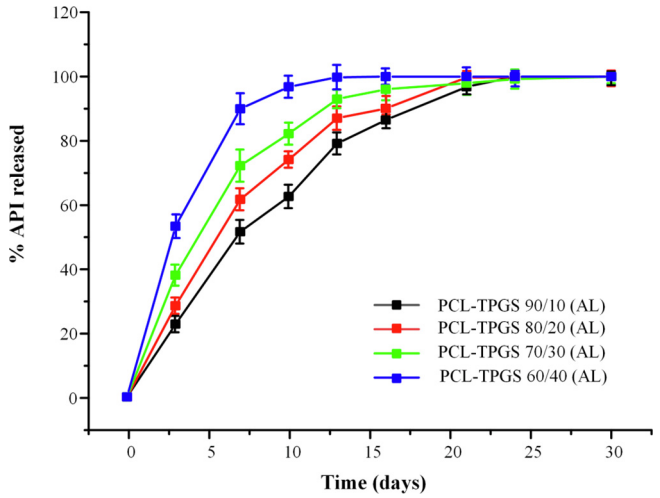

Fig. 8. *In vitro* release profiles of AL drug-loaded microspheres.

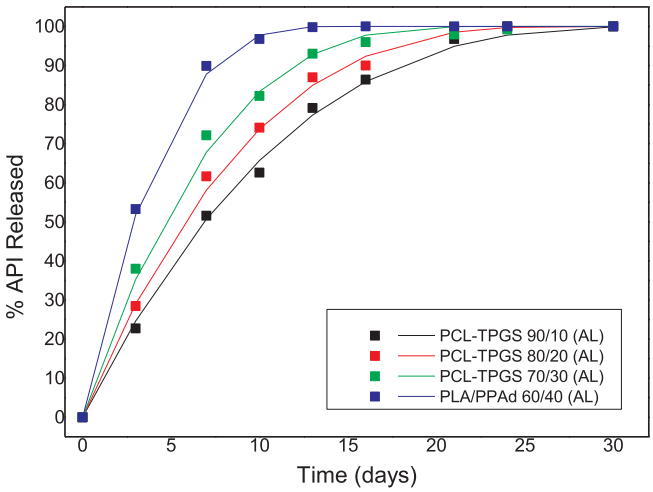

Fig. 9. Comparison between experimental (data points) and model release profiles (continuous lines).

content (such as those containing PCL-TPGS at a ratio of 90–10 w/w) showed a slow AL release rate, with approximately 20% of the API being released within the first three (3) days, while the 90% of the API was released after 21 days. The rest of the examined microspheres showed moderate release rates. Particularly, formulations containing PCL-TPGS in ratio of 80/20 w/w released almost 70% of the API in seven (7) days, while formulations containing PCL-TPGS 70/30 w/w released approximately 60% of the API at the same time interval. These differences among the prepared microspheres may be attributed to several factors, including water permeability and solubility within the polymer matrices, degree of crystallinity and crystalline morphology of copolymers and the API, microsphere particle size and size distribution, drug loading levels, melting points and glass transition temperatures of copolymers, and others. However, independently of all the above mentioned factors, it is clearly seen from the obtained results that, by varying the content of TPGS in the followed copolymerization process, several profiles of drug release may be obtained. This is a clear indication that the proposed system has a great ability to tune API's *in vitro* release properties, and hence, the in vivo API behavior.

3.2.7. Release data modeling

The two possible drug release mechanisms from the prepared microparticles are: 1) erosion (degradation) of the carrier (polymer) or 2) diffusion of the drug from the polymeric matrix (Korsmeyer et al., 1983). In the present study, since erosion experiments revealed the significant effect of polymer matrix erosion, any possible contribution of diffusion on the release mechanism of API can be estimated though *in vitro* release profile modeling. Initially, the *in vitro* release mechanism will be assumed to be controlled only from polymer erosion. This model is based on the following assumptions: (i) the drug is uniformly distributed in the polymer matrix (ii) the polymer is dissolved with a linear rate k (units of length per time). A simple analysis based on the conservation of polymer matrix volume leads to the following result for the percentage drug released (Parker et al., 2000):

$$\mathrm{Re}\,lease(\%) = 100\cdot(1-(1-kt/L_o)^n) \tag{6}$$

where, the exponent n is related to the geometry of the particles and L_o is the initial value of a characteristic particle size which evolves in time t as $L = L_o$-kt. The exponent n shows the dimensionality of the polymer particle shape and takes the values n = 1 for flakes, n = 2 for long cylinders and n = 3 for isotropic shapes. The exact shape is of no significance, since the value n = 3 holds for both spherical and cubical particles. The particles of the present work are clearly isotropic (see SEM analysis), so n can be safely assumed as 3. In this case, the characteristic dimension L can be considered equivalent to radius R of particles. Based on the above, Fig. 9 shows the results of Eq. (6) *in vitro* release profile fitting.

It is evident that the fitting curves lie within the error bars of the experimental points indicating that polymer erosion process is probably the only release mechanism for the prepared drug-loaded microspheres. The drug is completely immobile in the polymer matrix so diffusion has no contribution to the release process. The values of the ratio k/R_o extracted from the experimental data are (90/10) 0.03 day^{-1}, (80/20) 0.036 day^{-1}, (70/30) 0.045 day^{-1} (60/40) 0.072 day^{-1} where the polymer mixture composition appears in the parentheses. The extracted values of k/R_o can be considered as function of the percentage portion (P) of TPGS in the polymer mixture. A fitting procedure of the data leads to the following relation (in $days^{-1}$):

$$\frac{k}{R_o} = 2.5\cdot10^{-6}P^3 - 1.35\cdot10^{-4}P^2 + 2.9\cdot10^{-3}P + 0.012 \tag{7}$$

An estimation for the particle radius R_o (assuming an almost monodisperse particle size distribution) is needed to evaluate the linear release rate of the matrix k. For a value of R_o equal to 2 μm (based on Fig. 5 results) the release rate is approximately 0.1 μm/day. It is interesting to compare this with the enzymatic hydrolysis rate which is estimated from the Fig. 4 and is approximately 40 μm/day (i.e. increased by almost three orders of magnitude).

In the next step of API's *in vitro* release modelling, the developed model for monodispersed particle size distribution will be extended to cover arbitrary particle size distributions of isotropic geometry particles approximated as spheres. For this case f(r) is assumed to be the number density function of particles defined such as the product f(r)dr to be the number of particles with radius between r and r + dr. In order to work with dimensionless variables, the function f is normalized by the initial (before API's release begins) total number of particles N (i.e. F = f/N) and the radius r is normalized by the initial average radius of particles r_o (i.e. $\eta = r/r_o$). The new function $F(\eta,t)$ describes the evolution in time of the particle size distribution during *in vitro* release process. In particular, the initial function $F(\eta,0)$ is a probability density function and by construction its zero and first order moments take the value of unity. The evolution of the function F is described from the following population balance equation (Ramkrishna, 2000):

$$\frac{\partial F}{\partial t} - \frac{k}{r_o}\frac{\partial F}{\partial \eta} = 0 \tag{8}$$

The initial condition for this equation is $F(\eta,0) = F_o(\eta)$, where the function F_o refers to the distribution of polymer particles. The Eq. (8) is an hyperbolic partial differential equation and it can be solved in closed form, using the method of characteristics to give $F(\eta,t) = F_o(\eta + kt/r_o)$.

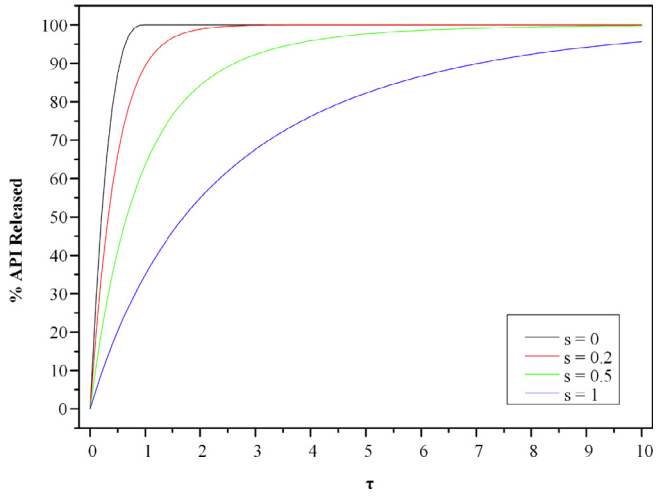

Fig. 10. Theoretical percentage drug released versus dimensionless time for several values of the dispersivity of the polymer particles size distribution.

As in the case of monodispersed particles, the percentage drug released is equal to the percentage of the dissolved polymer. This means that (using the new dimensional time variable $\tau = kt/r_o$ for clarity of presentation):

$$\text{Re}\,lease(\%) = 1 - \frac{\int_0^\infty \eta^3 F(\eta, \tau)d\eta}{\int_0^\infty \eta^3 F_0(\eta)d\eta} \quad (9)$$

Replacing the analytical solution for F in the integral at the numerator of the above equation and introducing the new integration variable $z = \eta + kt$ it is transformed to $\int_\tau^\infty (z-\tau)^3 F_0(z)dz$. This means that a numerical integration is needed for each value of time. To decrease the computational effort, the power term is expanded to give the following final expression for the release rate (requiring only four numerical integrations for the functions $M_i(\tau)$ with i = 0,1,2,3):

$$\text{Re}\,lease(\%) = 100\cdot(1 - \frac{M_3 - 3\tau M_2 + 3\tau^2 M_1 - \tau^3 M_0}{M_3(0)}) \quad (10)$$

where

$$M_i(\tau) = \int_\tau^\infty z^i F_0(z)dz \quad (11)$$

A very extensively used size distribution function for particulate processes is the so called log-normal one (Williams and Loyalka, 1991). The corresponding normalized function has the form

$$F_0(z) = \frac{1}{(2\pi s)^{1/2} z} \exp(-\frac{1}{2s}(\ln(z) + s/2)^2) \quad (12)$$

This function can reasonable approximate any realistic particle size distribution. The only parameter in the above normalized form of the size distribution is the so-called dispersivity "s" which is an index of the polydispersity of the distribution (it is zero for the monodisperse distribution and it increases as the polydispersity increases). According to the above the percentage drug release depends only on dimensionless time τ and on particle size polydispersity s. The integrals in Eq. (11) were computed numerically (by transformation to ordinary differential equations and implementing Euler method) to give the "universal" results of release shown in Fig. 10.

It is surprising that, not only the average particle size (i.e. r_o) but also the polydispersity (through s) has a major effect on release kinetics. The reason for this is that r_o is a number based average but the drug loading is proportional to the polymer particle volume. This implies that the release kinetics is dominated mainly by volumetric average of the particle size distribution. As polydispersity increases the ratio between volumetric and number based average radii increases and this leads to a delay of the release process. Fig. 9 can be used for the design and optimization of the release process. Having assessed experimentally the value of k as a function of the polymer particles composition (see Eq. (7)) one can reconstruct the release kinetics for arbitrary particle size distribution as it is described by its average radius and its dispersivity. In this way the release kinetics for any composition of PCL-TPGS particles (for TPGS fraction between 10% and 40%) and any particle size distribution can be computed allowing the development of a release profile suitable to any specified requirement.

4. Conclusion

In the present study AL drug-loaded PCL-TPGS microspheres were successfully prepared for the first time. The prepared PCL-TPGS copolymers were semi-crystalline in nature, while the content of TPGS significantly affected both intrinsic viscosity (increasing TPSG led to decreasing viscosity) and enzymatic hydrolysis (increasing TPSG led to increasing hydrolysis rate). Significant interactions (in the form of hydrogen bonds) were observed between the two components, while DSC analysis showed a significant melting point reduction with decreasing PCL content. AL was amorphously dispersed within the copolymer matrix (except in the case of high TPGS content), while no intermolecular interactions were observed between the API and the copolymers. *In vitro* release studies showed that the incorporation of TPGS can significantly control API's release rate (increasing rate was observed with increasing TPGS content). A detailed analysis of the release kinetic data allows the construction of a generalized model for drug release induced by polymer matrix erosion accounting for particle size distribution effect on the release kinetics.

References

Abou-Zeid, D.M., Muller, R.J., Deckwer, W.D., 2004. Biodegradation of aliphatic homopolyesters and aliphatic-aromatic copolyesters by anaerobic microorganisms. Biomacromolecules 5, 1687–1697.
Bae, J., Park, J.W., 2015. Preparation of an injectable depot system for long-term delivery of alendronate and evaluation of its anti-osteoporotic effect in an ovariectomized rat model. Int. J. Pharm. 480, 37–47.
Balas, F., Manzano, M., Horcajada, P., Vallet-Regi, M., 2006. Confinement and controlled release of bisphosphonates on ordered mesoporous silica-based materials. J. Am. Chem. Soc. 128, 8116–8117.
Bikiaris, D.N., Nianias, N.P., Karagiannidou, E.G., Docoslis, A., 2012. Effect of different nanoparticles on the properties and enzymatic hydrolysis mechanism of aliphatic polyesters. Polym. Degrad. Stab. 97, 2077–2089.
Bikiaris, D.N., Papageorgiou, G.Z., Giliopoulos, D.J., Stergiou, C.A., 2008. Correlation between chemical and solid-state structures and enzymatic hydrolysis in novel biodegradable polyesters. The case of poly(propylene alkanedicarboxylate)s. Macromol. Biosci. 8, 728–740.
Ciardelli, G., Chiono, V., Vozzi, G., Pracella, M., Ahluwalia, A., Barbani, N., Cristallini, C., Giusti, P., 2005. Blends of poly-(epsilon-caprolactone) and polysaccharides in tissue engineering applications. Biomacromolecules 6, 1961–1976.
Dolci, L.S., Panzavolta, S., Torricelli, P., Albertini, B., Sicuro, L., Fini, M., Bigi, A., Passerini, N., 2019. Modulation of Alendronate release from a calcium phosphate bone cement: an in vitro osteoblast-osteoclast co-culture study. Int. J. Pharm. 554, 245–255.
Dong, X., Zou, S., Guo, C., Wang, K., Zhao, F., Fan, H., Yin, J., Chen, D., 2018. Multifunctional redox-responsive and CD44 receptor targeting polymer-drug nanomedicine based curcumin and alendronate: synthesis, characterization and in vitro evaluation. Artif. Cells Nanomed. Biotechnol. 46, 168–177.
Duque, G., Rivas, D., 2007. Alendronate has an anabolic effect on bone through the differentiation of mesenchymal stem cells. J. Bone Mineral Res. Official J. Am. Soc. Bone Mineral Res. 22, 1603–1611.
Ezra, A., Hoffman, A., Breuer, E., Alferiev, I.S., Monkkonen, J., El Hanany-Rozen, N., Weiss, G., Stepensky, D., Gati, I., Cohen, H., Tormalehto, S., Amidon, G.L., Golomb, G., 2000. A peptide prodrug approach for improving bisphosphonate oral absorption. J. Med. Chem. 43, 3641–3652.
Fleisch, H., 2000. Bisphosphonates-clinical. In: Fleisch, H. (Ed.), Bisphosphonates in Bone Disease, Fourth Edition. Academic Press, San Diego, pp. 67–181.
Gaba, B., Fazil, M., Ali, A., Baboota, S., Sahni, J.K., Ali, J., 2015. Nanostructured lipid (NLCs) carriers as a bioavailability enhancement tool for oral administration. Drug Delivery 22, 691–700.
Gan, Z., Abe, H., Kurokawa, H., Doi, Y., 2001. Solid-state microstructures, thermal properties, and crystallization of biodegradable poly(butylene succinate) (PBS) and its copolyesters. Biomacromolecules 2, 605–613.
Guo, Y., Luo, J., Tan, S., Otieno, B.O., Zhang, Z., 2013. The applications of Vitamin E TPGS in drug delivery. Eur. J. Pharm. Sci. 49, 175–186.
Harada, M., Iida, K., Okamoto, K., Hayashi, H., Hirano, K., 2008. Reactive

compatibilization of biodegradable poly(lactic acid)/poly(ε-caprolactone) blends with reactive processing agents. Polym. Eng. Sci. 48, 1359–1368.
Hosny, K.M., 2016. Alendronate Sodium as Enteric Coated Solid Lipid Nanoparticles; Preparation, Optimization, and In Vivo Evaluation to Enhance Its Oral Bioavailability. PLoS ONE 11, e0154926.
Hughes, D.E., Wright, K.R., Uy, H.L., Sasaki, A., Yoneda, T., Roodman, G.D., Mundy, G.R., Boyce, B.F., 1995. Bisphosphonates promote apoptosis in murine osteoclasts in vitro and in vivo. Bone Mineral Res. Official J. Am. Soc. Bone Mineral Res. 10, 1478–1487.
Kim, C.W., Yun, Y.P., Lee, H.J., Hwang, Y.S., Kwon, I.K., Lee, S.C., 2010. In situ fabrication of alendronate-loaded calcium phosphate microspheres: controlled release for inhibition of osteoclastogenesis. J. Controlled Release Official J. Controlled Release Soc. 147, 45–53.
Korsmeyer, R.W., Gurny, R., Doelker, E., Buri, P., Peppas, N.A., 1983. Mechanisms of solute release from porous hydrophilic polymers. Int. J. Pharm. 15, 25–35.
Lin, J.H., 1996. Bisphosphonates: a review of their pharmacokinetic properties. Bone 18, 75–85.
Lin, J.H., Chen, I.W., deLuna, F.A., 1994. On the absorption of alendronate in rats. J. Pharm. Sci. 83, 1741–1746.
Luo, Z., Wu, L., Xie, C., Xiao, X., 2018. Amino-Modified Polylactic Acid Nanofibre Microspheres as Drug Sustained Release Carriers for Alendronate AU - Chen, Shunyu. Polymer-Plastics Technol. Eng. 57, 1873–1881.
Marten, E., Müller, R.-J., Deckwer, W.-D., 2003. Studies on the enzymatic hydrolysis of polyesters I. Low molecular mass model esters and aliphatic polyesters. Polym. Degrad. Stab. 80, 485–501.
Miladi, K., Sfar, S., Fessi, H., Elaissari, A., 2013. Drug carriers in osteoporosis: preparation, drug encapsulation and applications. Int. J. Pharm. 445, 181–195.
Miller, K., Clementi, C., Polyak, D., Eldar-Boock, A., Benayoun, L., Barshack, I., Shaked, Y., Pasut, G., Satchi-Fainaro, R., 2013. Poly(ethylene glycol)-paclitaxel-alendronate self-assembled micelles for the targeted treatment of breast cancer bone metastases. Biomaterials 34, 3795–3806.
Miyazaki, T., Inoue, T., Shirosaki, Y., Kawashita, M., Matsubara, T., Matsumine, A., 2014. Bisphosphonate release profiles from magnetite microspheres. J. Biomater. Appl. 29, 543–547.
Mondal, T., Sunny, M.C., Khastgir, D., Varma, H.K., Ramesh, P., 2012. Poly (l-lactide-co-Є caprolactone) microspheres laden with bioactive glass-ceramic and alendronate sodium as bone regenerative scaffolds. Mater. Sci. Eng., C 32, 697–706.
Nafea, E.H., El-Massik, M.A., El-Khordagui, L.K., Marei, M.K., Khalafallah, N.M., 2007. Alendronate PLGA microspheres with high loading efficiency for dental applications. J. Microencapsul. 24, 525–538.
Nafee, N., Zewail, M., Boraie, N., 2018. Alendronate-loaded, biodegradable smart hydrogel: a promising injectable depot formulation for osteoporosis. J. Drug Target. 26, 563–575.
Nanaki, S., Barmpalexis, P., Iatrou, A., Christodoulou, E., Kostoglou, M., Bikiaris, D.N., 2018a. Risperidone Controlled Release Microspheres Based on Poly(Lactic Acid)-Poly (Propylene Adipate) Novel Polymer Blends Appropriate for Long Acting Injectable Formulations. Pharmaceutics 10, 130.
Nanaki, S., Barmpalexis, P., Papakonstantinou, Z., Christodoulou, E., Kostoglou, M., Bikiaris, D.N., 2018b. Preparation of New Risperidone Depot Microspheres Based on Novel Biocompatible Poly(Alkylene Adipate) Polyesters as Long-Acting Injectable Formulations. J. Pharm. Sci. 107, 2891–2901.
Nanaki, S.G., Pantopoulos, K., Bikiaris, D.N., 2011. Synthesis of biocompatible poly(ε-caprolactone)- block-poly(propylene adipate) copolymers appropriate for drug nanoencapsulation in the form of core-shell nanoparticles. Int. J. Nanomed. 6, 2981–2995.
Nerantzaki, M., Skoufa, E., Adam, K.-V., Nanaki, S., Avgeropoulos, A., Kostoglou, M., Bikiaris, D., 2018. Amphiphilic Block Copolymer Microspheres Derived from Castor Oil, Poly(ε-carpolactone), and Poly(ethylene glycol): Preparation, Characterization and Application in Naltrexone Drug Delivery. Materials (Basel, Switzerland) 11, 1996.
Neuzil, J., Dong, L.-F., Ramanathapuram, L., Hahn, T., Chladova, M., Wang, X.-F., Zobalova, R., Prochazka, L., Gold, M., Freeman, R., Turanek, J., Akporiaye, E.T., Dyason, J.C., Ralph, S.J., 2007. Vitamin E analogues as a novel group of mitocans: anti-cancer agents that act by targeting mitochondria. Mol. Aspects Med. 28, 607–645.
Nishikawa, M., Akatsu, T., Katayama, Y., Yasutomo, Y., Kado, S., Kugal, N., Yamamoto, M., Nagata, N., 1996. Bisphosphonates act on osteoblastic cells and inhibit osteoclast formation in mouse marrow cultures. Bone 18, 9–14.
Parker, A., Vigouroux, F., Reed, W.F., 2000. Dissolution kinetics of polymer powders. AIChE J. 46, 1290–1299.
Qiu, Z., Ikehara, T., Nishi, T., 2003. Poly(hydroxybutyrate)/poly(butylene succinate) blends: miscibility and nonisothermal crystallization. Polymer 44, 2503–2508.
Qu, G.X., Ying, Z.M., Zhao, C.C., Yan, S.G., Cai, X.Z., 2018. Mechanical Properties and Porosity of Acrylic Cement Bone Loaded with Alendronate Powder. Int. J. Med. Sci. 15, 1458–1465.
Ramkrishna, D., 2000. Theory and Applications to Particulate Systems in. Engineering.
Rhim, S.Y., Park, J.H., Park, Y.S., Lee, M.H., Kim, D.S., Shaw, L.M., Yang, S.C., Kang, J.S., 2009. Bioavailability and bioequivalence of two oral formulations of alendronate sodium 70 mg: an open-label, randomized, two-period crossover comparison in healthy Korean adult male volunteers. Clin. Ther. 31, 1037–1045.
Sahni, M., Guenther, H.L., Fleisch, H., Collin, P., Martin, T.J., 1993. Bisphosphonates act on rat bone resorption through the mediation of osteoblasts. J. Clin. Investig. 91, 2004–2011.
Samdancioglu, S., Calis, S., Sumnu, M., Atilla Hincal, A., 2006. Formulation and in vitro evaluation of bisphosphonate loaded microspheres for implantation in osteolysis. Drug Dev. Ind. Pharm. 32, 473–481.
Sharpe, M., Noble, S., Spencer, C.M., 2001. Alendronate: an update of its use in osteoporosis. Drugs 61, 999–1039.
Siafaka, P.I., Üstündağ Okur, N., Mone, M., Giannakopoulou, S., Er, S., Pavlidou, E., Karavas, E., Bikiaris, D.N., 2016. Two Different Approaches for Oral Administration of Voriconazole Loaded Formulations: Electrospun Fibers versus β-Cyclodextrin Complexes. Int. J. Mol. Sci. 17, 282–283.
Solomon, O.F., Ciută, I.Z., 1962. Détermination de la viscosité intrinsèque de solutions de polymères par une simple détermination de la viscosité. J. Appl. Polym. Sci. 6, 683–686.
Umeki, N., Sato, T., Harada, M., Takeda, J., Saito, S., Iwao, Y., Itai, S., 2010. Preparation and evaluation of biodegradable microspheres containing a new potent osteogenic compound and new synthetic polymers for sustained release. Int. J. Pharm. 392, 42–50.
Wang, C.Z., Chen, S.M., Chen, C.H., Wang, C.K., Wang, G.J., Chang, J.K., Ho, M.L., 2010. The effect of the local delivery of alendronate on human adipose-derived stem cell-based bone regeneration. Biomaterials 31, 8674–8683.
Williams, M.M.R., Loyalka, S.K., 1991. Aerosol Science: Theory and. Practice Pergamon Press.
Wright, J.E.I., Gittens, S.A., Bansal, G., Kitov, P.I., Sindrey, D., Kucharski, C., Uludağ, H., 2006. A comparison of mineral affinity of bisphosphonate–protein conjugates constructed with disulfide and thioether linkages. Biomaterials 27, 769–784.
Wu, H., Xu, Y., Liu, G., Ling, J., Dash, B.C., Ruan, J., Zhang, C., 2014. Emulsion cross-linked chitosan/nanohydroxyapatite microspheres for controlled release of alendronate. Journal of materials science. Materials in medicine 25, 2649–2658.
Yang, C., Wu, T., Qi, Y., Zhang, Z., 2018. Recent Advances in the Application of Vitamin E TPGS for Drug Delivery. Theranostics 8, 464–485.
Yang, H., Gao, H., Wang, Y., 2016. Hollow hydroxyapatite microsphere: a promising carrier for bone tissue engineering. J. Microencapsul. 1–6.
Yuan, M., Wang, Y., Li, X., Xiong, C., Deng, X., 2000. Polymerization of Lactides and Lactones. 10. Synthesis, Characterization, and Application of Amino-Terminated Poly (ethylene glycol)-co-poly(ε-caprolactone) Block Copolymer. Macromolecules 33, 1613–1617.
Zhang, H., Liu, G., Zeng, X., Wu, Y., Yang, C., Mei, L., Wang, Z., Huang, L., 2015. Fabrication of genistein-loaded biodegradable TPGS-b-PCL nanoparticles for improved therapeutic effects in cervical cancer cells. Int. J. Nanomed. 10, 2461–2473.
Zhang, Z., Tan, S., Feng, S.S., 2012. Vitamin E TPGS as a molecular biomaterial for drug delivery. Biomaterials 33, 4889–4906.
Zorba, T., Chrissafis, K., Paraskevopoulos, K.M., Bikiaris, D.N., 2007. Synthesis, characterization and thermal degradation mechanism of three poly(alkylene adipate)s: comparative study. Polym. Degrad. Stab. 92, 222–230.